

El Niño Enhances Snowline Rise and Ice Loss on the Quelccaya Ice Cap, Peru

Kara A. Lamantia^{1,2}, Laura J. Larocca³, Lonnie G. Thompson^{1,2}, Bryan G. Mark^{1,4}

¹ Byrd Polar and Climate Research Center, Ohio State University, Columbus, OH, USA

5 ² School of Earth Sciences, Ohio State University, Columbus, OH, USA

³ School of Ocean Futures, Arizona State University, Tempe, AZ, USA

⁴ Department of Geography, Ohio State University, Columbus, OH, USA

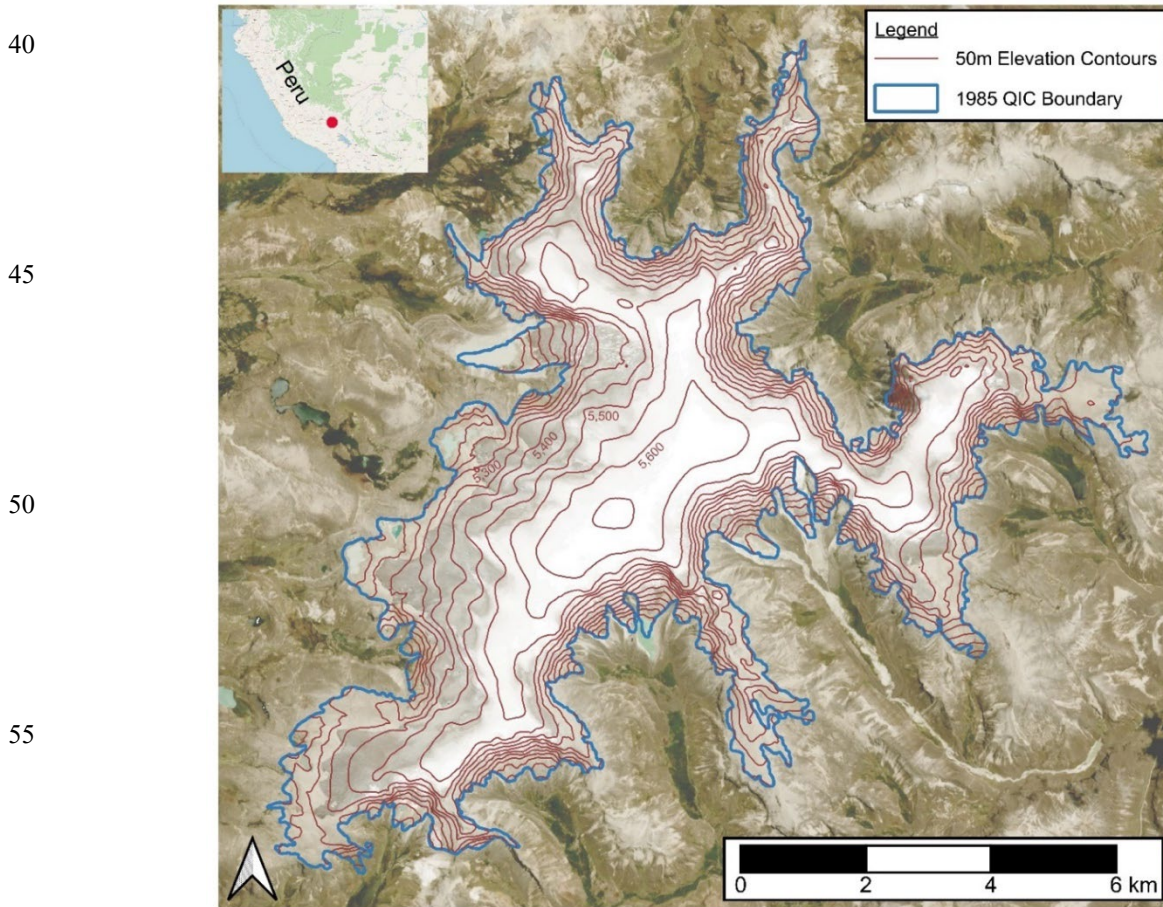
Correspondence to: Kara A. Lamantia (lamantia.31.@osu.edu)

Abstract. Tropical glaciers in the central Andes are vital water resources and crucial climate indicators, currently undergoing rapid retreat. However, understanding their vulnerability to the combined effects of persistent warming, short-term climate phenomena, and interannual fluctuations remains limited. Here we automate the mapping of key mass balance parameters on the Quelccaya Ice Cap (QIC) in Peru, one of the largest tropical ice caps. Using Landsat's near-infrared (NIR) band, we analyze snow cover area (SCA) and total area (TA) and calculate the Accumulation Area Ratio (AAR) and Equilibrium Line Altitude (ELA) over nearly 40 years (1985-2023). Between 1985 and 2022, the QIC lost ~58% and ~37% of its SCA and TA, respectively. We show that the QIC's reduction in SCA and rise in ELA are exacerbated by El Niño events, which are strongly correlated to the preceding wet season's Ocean Niño Index (ONI). Further, expansion in the QIC's SCA is observed during all La Niña years, except for the 2021-2022 La Niña. Although a singular event, this could suggest an inability for SCA recovery and accelerated decline into the future, driven primarily by anthropogenic warming.

1 Introduction

20 Tropical glaciers are known to be especially sensitive to climate shifts (Kaser & Osmaston, 2002) and their accelerated decline has been well-documented in recent decades (Bradley et al., 2006; Braun et al., 2019; Hanshaw & Bookhagen, 2014; Hugonnet et al., 2021; Pepin et al., 2015, 2022; Seehaus et al., 2020; Thompson et al., 2011, 2021; Vuille et al., 2015). In the low latitudes, glaciers are projected to lose ~69-98% of their 2015 mass by 2100, depending on the emissions scenario (i.e., RCP2.6 and RCP 8.5, respectively; Rounce et al., 2023). The freezing level height in the tropics is affected on an interannual basis by El Niño Southern Oscillation (ENSO) variations and follows the Multivariate ENSO Index (MEI) on a year-to-year basis (Bradley et al., 2009; Favier et al., 2004; Thompson, 2000; Vuille et al., 2000). The decline of the Quelccaya Ice Cap (QIC; Fig. 1), located in the Cordillera Vilcanota (CV) range in the outer tropical region of the Andes, is one such concern with worst case (RCP8.5) projections suggesting the 'point of no return' (i.e., the rise of the ELA above the summit) as early as 2050 (Yarleque et al., 2018), leaving QIC a wasting ice field, similar to Kilimanjaro. Contemporary changes in the QIC's outlet glaciers have been monitored frequently (Brecher & Thompson, 1993) and contextualized within a longer, millennial-scale timeframe (e.g.,

Mark et al., 2002; Lamantia et al., 2023). For example, Mark et al. (2022) combine moraine chronology with digital topography to model deglaciation rates during the Last Glaciation and Holocene and find that the QIC's most rapid retreat has occurred over recent centuries (Mark et al., 2002). Further, radiocarbon-dated plant remains from the QIC ice margin suggest that the ice cap's retracted present-day extent has not occurred in the last 7,000 years (Lamantia et al., 2023). In addition, the QIC's high-resolution ice-core records have proven invaluable for understanding past climatic and environmental variability in the region (Thompson, 2000; Thompson et al., 1985, 2013, 2017, 2021). Thus, the ongoing loss of tropical glaciers will not only impact local communities that depend on glacial meltwater but has implications for the preservation of long-term climate records, essential for assessing the rate and magnitude of current changes (Thompson et al., 2021).



60 **Figure 1:** Aerial view of the Quelccaya Ice Cap ($13^{\circ}56'S$; $70^{\circ}50'W$) from October 11, 2023. The summit of the QIC reaches 5,670 m a.s.l with a handful of outlet glaciers to the west and a steep-sided eastern portion. Base Imagery was obtained from Planet Labs Dove Satellite with 3-meter resolution and inset (top left) was obtained from the OpenStreetMap database (© OpenStreetMap contributors 2023. Distributed under the Open Data Commons Open Database License (ODbL) v1.0.)

In the tropics, there is no seasonal snow cover beyond the glacierized area that would provide an additional buffer to the ice cap's decline (Vuille et al., 2018). Quelccaya's snowfall is largely controlled by the South American Summer Monsoon

(SAMS) with the snowfall peak in December and moisture transport from the Amazon is influenced by ENSO variations (J. V. Hurley et al., 2015). There has been no significant change in precipitation around the QIC over the last fifty years, with 10% of stations in the CV recording only a slight decrease in rainfall (Casimiro et al., 2013). However, ice core records from the QIC core reveal the net accumulation in the region has been above average for the last century (Thompson L.G., 2017). In the Peruvian Amazon–Andes basin, mean annual temperature has increased by $\sim 0.09^{\circ}\text{C}$ per decade over the last sixty years, while maximum summer temperature time series in the Andes show an even higher magnitude trend (0.15°C per decade; Casimiro et al., 2013). Additionally, ice cores from multiple locations in Peru document this accelerating enrichment (Thompson, 2017; Thompson et al., 2013). Nearby mountain ranges such as the Cordillera Blanca and Real have experienced an increase in the freezing level height (FLH) by 160 m over the last five and a half decades with implications for not only where snow can survive and accumulate (Bradley et al., 2009; Schauwecker et al., 2014; Seehaus et al., 2020) but also increased albedo in the ablation zone influenced by a rise of the rain/snow line (Rabatel et al., 2013). High-resolution ice core records show that the QIC is an excellent recorder of El Niño events that create elevated sea surface temperatures (SSTs) in the Eastern Pacific Ocean, recording years of strong El Niño events with isotopically enriched $\delta^{18}\text{O}$ (Thompson et al., 2011, 2017). Alongside these ice core records, the QIC’s contemporary and past margins have been monitored and reconstructed, but its sensitivity and response to multiple short-term climate phenomena over recent decades have yet to be extensively evaluated. Thus, the QIC is an ideal setting to assess the combined effects of sustained warming and short-term climate variations, such as ENSO, on tropical glacier vulnerability.

Since routine ground-based measurements in a remote location such as south-central Peru are difficult to maintain, using satellite imagery to estimate the Equilibrium Line Altitude (ELA) has become a viable solution for long-term glacier monitoring. Previous studies have shown that the end of dry season (September) location of the snowline altitude (SLA) can act as a proxy for the ELA and ultimately be used to infer the mass balance of a glacier or ice cap (Fang et al., 2011; Hu et al., 2020; Liu et al., 2021; Racoviteanu et al., 2019). Initial studies in the Andes involved a manual assessment of the Artesonraju and Zongo glaciers via Landsat and SPOT imagery compared against field measurements (Rabatel et al., 2012). Yarleque et al., (2018) most recently analyzed the QIC’s response to warming scenarios based on the FLH/ELA relationship and future ELA projections. Here, we employ cloud-based analysis of satellite imagery to assess the QIC at the end of the dry season between 1985 and 2023. We automate not only the detection of the snow-covered area (SCA) and total area (TA), but also the calculation of the accumulation area ratio (AAR), the median elevation of the SCA, and the SLA as a proxy for the ELA. Changes to the ELA, SCA, and AAR are analyzed alongside ERA5–Land Reanalysis Climate Data from the European Centre for Medium Weather Range Weather Forecast (ECMWF) including total precipitation and surface temperature as well as multiple ENSO Indices including the MEI, the Ocean Niño Index (ONI), and the Southern Oscillation Index (SOI). We focus on the strongest most recent El Niño events (1998, 2016, and 2023) and the QIC’s response to these short-term climate anomalies.

2 Methods

100 2.1 Current Analysis Techniques

Manual snowline tracing is often limited to high quality imagery to discern between snow and ice. However, recent advances in image analysis have allowed for the automation of snowline detection via satellite imagery. Typically, a suite of images, often from Landsat satellites, are paired with one or more Digital Elevation Models (DEMs) and a glacier outline within the temporal scale of interest (Li et al., 2022). From there, a variety of thresholds are evaluated and set for the area of interest to
105 separate snow from ice, and extract the position of the transition (Racoviteanu et al., 2019). There are challenges in this process including the adjustment of surface reflectance for varying topographies, occurrence of patchy snow cover on the glacier surface, and highly variable atmospheric conditions that require the algorithm to be customized for the location of interest (Racoviteanu et al., 2019). Previous studies on Andean glaciers have used a handful of techniques to extract the location of the
110 snowline and to overcome some of the aforementioned challenges, including spectral mixing analysis, simple band ratios and filtering, hillshade mask shadow removal, and manual editing (Hanshaw & Bookhagen, 2014; Klein & Isacks, 1999). Here we implement an automated approach that employs a topographic correction, followed by segmentation of the NIR band via the OTSU method, which we describe in further detail in section 2.3, below.

2.2 Data Collection

To automate the SCA detection and ELA calculation, the following data inputs were required: an annual satellite image, a
115 DEM, and the 1985 outline of the QIC. Using the Google Earth Engine platform (GEE) we selected annual Landsat images as close as possible to September 15th with clear visibility of the QIC from 1985 to 2023 (Table S1). Mid to end September marks the end of the dry season in the CV, which enabled analysis of the ice cap without extraneous snowfall around the perimeter. Imagery from each year was on average ± 23 days within the target date and was manually inspected to ensure no recent snowfall events occurred. If September imagery was not available, October and November images were collected, and if
120 imagery was still not available August and July were collected with the intention to collect the closest to end of dry season conditions at the QIC. No images were used if a recent snowfall event was evident. Sentinel-2 imagery was used in 2021 and 2023, due to a lack of cloudless images from Landsat 8/9. Separate scripts were adapted for each satellite (i.e., Landsat or Sentinel-2). We note that the 2023 results are not included in our initial analysis of QIC's ELA change as it is part of an incomplete El Niño event. No imagery was collected for the years 1987, 1993, 2004, 2012, and 2018 due to high cloud cover
125 and/or visible snowfall events. We used two DEMs to account for changes in ice elevation over time and any down wasting of the QIC. Initially the NASADEM, created from the Shuttle Radar Topography Missions (SRTM), was implemented from 1985 to 2005. Post 2005, the COP30 DEM, released in 2010, was implemented following an assessment of surface differences in both DEMs between 2005 to 2015. Additionally, throughout and following the two largest El Niño events (1997-1999 and 2015-2017), multiple images (16 and 18, respectively) were collected, from June of the first year to November of the last year,
130 to assess short-term change and response of the QIC to El Niño events.

2.3 Satellite Analysis for Snow Cover Area

To begin, the least cloudy image from the target year closest to the end of dry season is clipped to the region of interest (ROI), the delineated QIC boundary (Step 1; Fig. S1). Pre-processing of each image included calculating the slope and aspect of the ROI from the DEM (Step 2). We implemented the Ekstrand Correction (Ekstrand, 1996) to account for topographic effects such as shadowing due to differences in sun elevation and incidence angle (Step 3) rather than a pixel-based Minnaert Correction method (Ge et al., 2008) which resulted in the over-correction of the steeper eastern side of the QIC. To delineate the snow cover area (SCA), the NIR band was assessed with an image segmentation algorithm, the OTSU method (Gaddam et al., 2022). This results in a bimodal frequency histogram where an automatically detected threshold separates snow from ice (Step 4; Fig. S2). Once calculated, it is applied to the NIR band to create a binary mask of snow and ice (Step 4). The annual image and DEM are then clipped to the snow mask creating the SCA, and the DEM data is extracted (Step 5). Following this, the SCA is calculated based on the number of pixels and image resolution, and the median elevation of the SCA is determined. SCAs are exported to shapefiles and the DEM data is exported as a histogram in 50-meter elevation bins (Step 6).

2.3 Calculation of Total Area, AAR, and ELA, and Uncertainty

As the SLA is a proxy for the ELA, we will use the term ELA from this point forward. In pursuit of the ELA, we calculated the Accumulation Area Ratio (AAR). The AAR is defined as: $AAR = A_c / (A_c + A_b)$ where A_c is the accumulation area, A_b is the ice covered area, and $A_c + A_b$ is the total area (TA) (Meier, 1962). In this case, A_c is the SCA and $A_c + A_b$ is the TA (both ice and snow). To calculate the TA, we automated the calculation of the Normalized Difference Snow Index (NDSI), which leverages the reflectance of snow and ice in the green and SWIR spectra compared to other land cover types. The NDSI is calculated by the following equation: $NDSI = (\rho_G - \rho_{SWIR}) / (\rho_G + \rho_{SWIR})$, where ρ_G and ρ_{SWIR} are the reflectance of the green and shortwave infrared bands, respectively (Dozier, 1989; Hall & Riggs, 2007). We used the same OTSU thresholding method to calculate the NDSI threshold, typically set around 0.4 (Dozier, 1989; Hall & Riggs, 2007; Sankey et al., 2015). The number of snow- and ice-covered pixels is multiplied by the appropriate pixel resolution to obtain the TA. By applying the threshold to each image, we obtained a binary image of snow and ice versus land cover and used this to calculate the TA (Step 7). The AAR is calculated by dividing the SCA by the TA (Step 8). The ELA is calculated using the DEM and the AAR by taking the $1 - AAR$ percentile of all elevations in the TA (Step 9; Fig. S3). For example, if the AAR is 0.8, we assume the ELA is located at the 20th percentile of elevations in the TA. In summary, for each image analyzed, we obtained the SCA, the median elevation, the TA, the AAR, and the ELA. Calculated results for the SCA and TA via our automated methods are in good agreement with manual digitizations (within $\pm 3\%$). Other studies have shown automated detection of snowlines produce similar results to manual digitization and low level of error (Hanshaw & Bookhagen, 2014) with automated detection being preferable to manual as repetition is simpler and any error is likely to be more consistent (Paul et al., 2013).

2.4 Reanalysis Data and ENSO Correlation

To compare the QIC's SCA and ELA with climate, we used daily and monthly averaged ERA5–Land Reanalysis Climate Data from the European Centre for Medium-Range Weather Forecasts (ECMWF), including total precipitation and 550mb temperature. Initially, we divided the data into wet (October to April) and dry (May to September) seasons based on precipitation records and past literature (Kaser & Osmaston, 2002; Veettil et al., 2017). To observe changes in climate at the QIC over time we calculated the average precipitation and temperature in five-year intervals, and the average number of days above and below freezing for each season from 1985 to 2023. Finally, to assess the QIC's interannual response to climatic anomalies we paired detrended ELA, SCA, and median elevation with the MEI, SOI, and ONI indices for correlation. As such, the variables for each year were correlated with the preceding months' indices, one year before the annual September observation date.

3 Results

3.1 Ice Loss and Multi-Decadal Climate Trends

Over the observation period (1985 to 2022), the QIC lost ~37% of its TA and ~58% of its SCA (1985: TA=~58.7 km², SCA=~46.3 km²; 2022: TA=~36.7 km², SCA=~19.7 km²; Table S2). Between the first and last five years of observation, the QIC's SCA and TA declined by ~38% and ~29%, respectively. This TA loss is concurrent with a retreat of the SCA to higher elevations (Fig. 2). We observed a 209 m and 112 m rise of the ELA and median elevation of the SCA, respectively. In 1985, 90% of the SCA existed above 5,250 m a.s.l., and in 2021, 90% of the SCA shifted to elevations above 5,350 m a.s.l. Further, by 2022, 90% of the SCA shifted even higher, to elevations above 5,400 m a.s.l. On average, the SCA and TA decreased by ~0.72 km² and ~0.59 km² per year, with an average yearly ELA rise of ~5.65m. Linear regression models suggest a loss of 0.47±0.09 km² yr⁻¹ (R²=0.44, p<0.001) in the QIC's SCA; a loss of 0.49±0.02 km² yr⁻¹ (R²=0.93, p<0.001) in the QIC's TA; and an average rise of 3.61±0.79 m yr⁻¹ (R²=0.40, p<0.001) in the QIC's ELA. However, the removal of the three largest El Niño years (1998, 2016, and 2023) resulted in slower average losses in QIC's SCA, and a slower average rise in QIC's ELA: -0.42±0.07 km² yr⁻¹ (R²=0.58, p<0.001); and +3.25±0.64 m yr⁻¹ (R²=0.47, p<0.001), respectively (Table S3). The QIC's average AAR (not including El Niño and La Niña years) is 0.74 over the study period. Conversely, during the strongest El Niño years (1998, 2016, and 2023) the QIC's AAR was 0.32, 0.40, and 0.52, respectively and during the strongest La Niña years (1999 and 2011) the QIC's AAR was 0.83, and 0.82.

Daily and monthly variations recorded at the QIC summit and bottom margin weather stations from Bradley et al., (2009) are well correlated with the ERA5 550mb temperature dataset, which was used to determine changes in temperature through the observation period. Between the first and last five years in our observational period, the reanalysis data recorded a 0.60°C increase in wet season (October-April) temperature and a 1.14°C increase in dry season (May – September) temperature.

Similarly, the number of days above 0°C rose from 1% to 6% in the wet season and from 0.5% to 8% in the dry season between the first five and last five years. These results are consistent with previous studies that suggest a ~0.1°C/decade rise in upper air temperature, and a rise in the height of the freezing level (~45 m between 1977-2007) in the tropics near the QIC (Bradley et al., 2009; Vuille et al., 2008). We observe no significant change in precipitation in both the wet and dry seasons (wet: $R^2=0.02$, $p=0.05$; dry: $R^2=0.03$, $p=0.01$) with 73% of the precipitation occurring during the wet season.

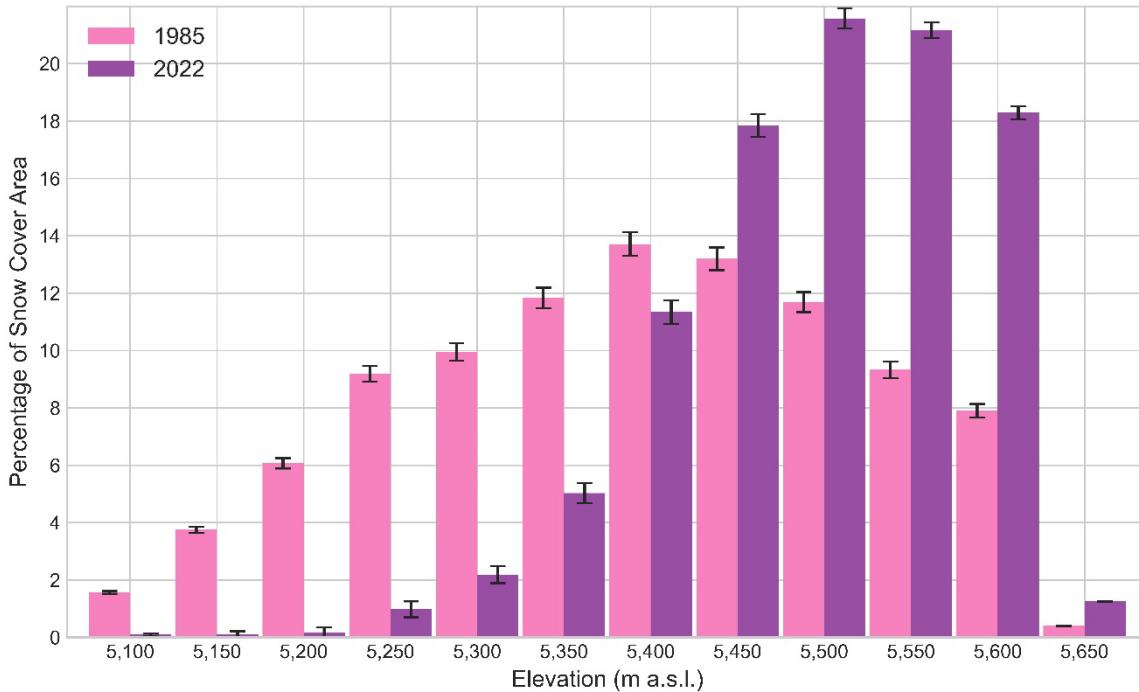


Figure 2: Percentage of snow cover area (SCA) in 50-meter elevation bins, demonstrating the shift to higher elevations.

215 3.2 QIC Response to Short-Term Climate Phenomena

The strongest El Niño events (1998, 2016, and 2023) coincide with a large decrease in the QIC’s SCA. We observed a 59% reduction in SCA from 1997 to 1998 and a 48% reduction from 2015 to 2016. In 1999, a rebound of the SCA was observed back to 1997 conditions however, in 2017 the SCA only reached about 76% of its 2015 value (~32km²) following the 2016 El Niño (Fig. 3). A small increase in the SCA is observed in 2019 (no imagery was available for 2018), however, to date the SCA has not returned to its pre-El Niño 2015 extent and has continued to decline through 2022. To better determine QIC changes during the El Niño events, high frequency sampling was conducted around the complete El Niño events, consisting of 16 and 18 images collected between 1997–1999 and 2015–2017, respectively. In both cases, the lowest SCA during El Niño is observed in the annual mid-September measurement, with a steady decline occurring from the prior year’s September measurement over the three consecutive years. In addition, correlation between the monthly ELA and monthly ONI index

225 during the two El Niño events (1997-1999 and 2015-2017) are 0.68 and 0.26, respectively. The QIC's AAR decreased from
0.71 to 0.31 from 1997 to 1998 and from 0.76 to 0.41 from 2015 to 2016. During these El Niño events, ERA5 data shows
increased air temperatures while precipitation patterns and magnitude remain largely unchanged. For instance, during the dry
season from 1997 to 1998 there is a 1.35°C increase in temperature and a change in total precipitation of less than 0.02 meters.
Additionally, linear regression models for ELA and SCA that include El Niño as a binary predictor (i.e., yes or no) improve
230 the R² values from 0.39 to 0.67 (p<0.001) and 0.44 to 0.72 (p<0.001), respectively. Conversely, the R² value for the model
predicting TA does not improve with the inclusion of the binary predictor. An analysis of variance (ANOVA) with a post hoc
test shows a significant difference in the mean SCA and ELA between El Niño and neutral years, in the AAR between El Niño
and neutral years and between El Niño to La Niña years (Fig S4). There is no significant difference in the mean TA between
El Niño, La Niña, and neutral years (Table S4). As the 2023 measurements occur during an ongoing El Niño event, we initially
235 compiled data from 1985 to 2022 and report the 2023 data as an additional insight into the effects of El Niño on the QIC. If
we consider the 2023 El Niño, between 1985 to 2023, we observed a 61% decline in the QIC's SCA in just under 40 years
(Fig. 4). The QIC's SCA during the onset of the 2023 El Niño is ~17.97 km²—a 9% loss compared to that of 2022. The 2023
AAR is 0.53, well below the average (i.e. 0.74), and from 2022 to 2023, we observed a 15 m and 8 m rise of the ELA and
median elevation.

240 ENSO indices are most strongly correlated with the QIC's ELA, SCA, and median elevation as they best represent the changing
ice distribution and mass. We evaluated all three previously mentioned ENSO indices but have chosen to discuss the ONI as
it presented the clearest patterns between ENSO and the assessed QIC variables (Table S5). The ONI is measured as sea surface
temperature (SST) anomalies in the Niño 3.4 zone (5°N - 5°S and 120°W – 170°W) and is used to define El Niño and La Niño
events. The ONI is most strongly correlated to the median elevation (Fig. 5) with a Pearson coefficient from the preceding
245 April back through the previous September ranging from 0.46 to 0.61 (P<0.05). The ONI and ELA are similarly positively
correlated (0.41 to 0.58 April-September), while the ONI index and SCA exhibit a negative correlation of similar strength
April through September (-0.44 to -0.60).

250

255

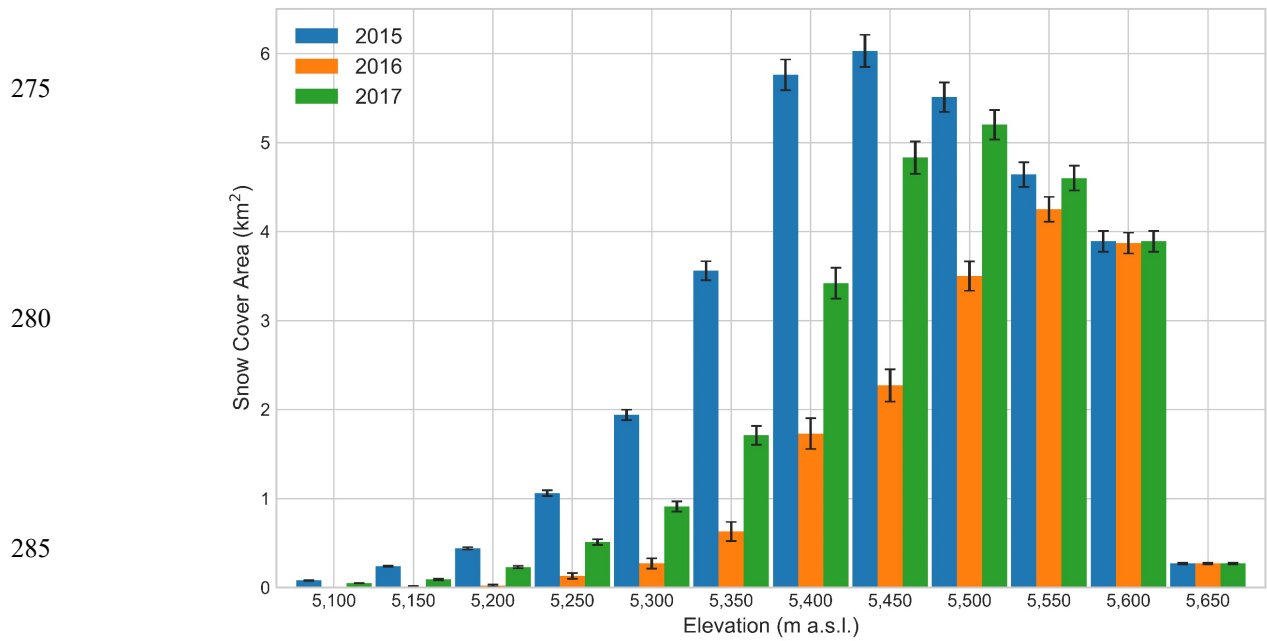
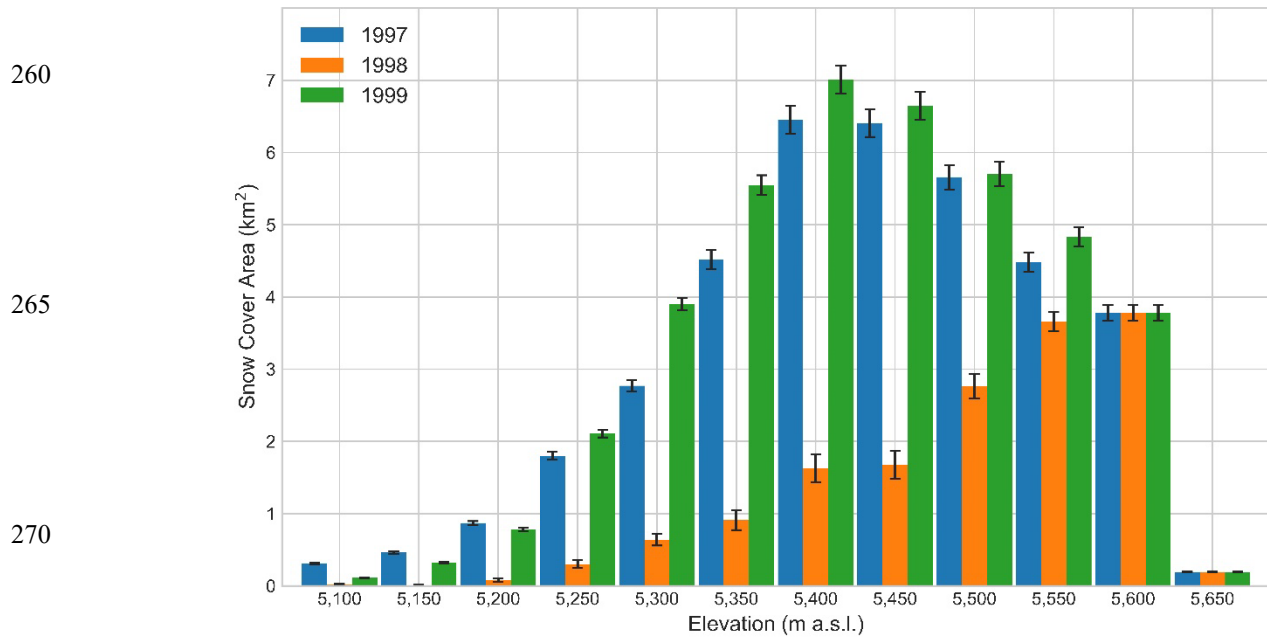


Figure 3: Percentage of snow cover displaying reduction and rebound of the SCA during the 1998 El Niño event (top) and incomplete recovery following the 2016 El Niño event (bottom).

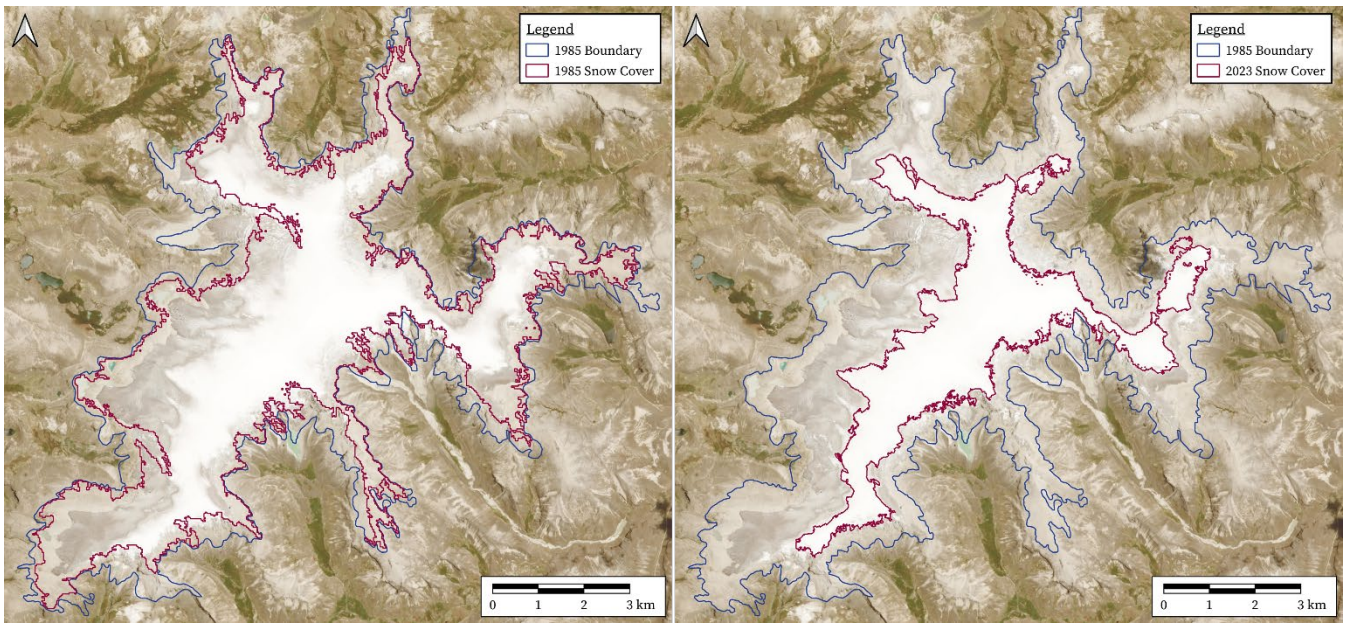


Figure 4: Decrease in the QIC's SCA (red) and TA (blue) at the end of the dry season from 1985 (left) to 2023 (right). Base Imagery obtained from Planet Labs Dove Satellite with 3-meter resolution, October 2023.

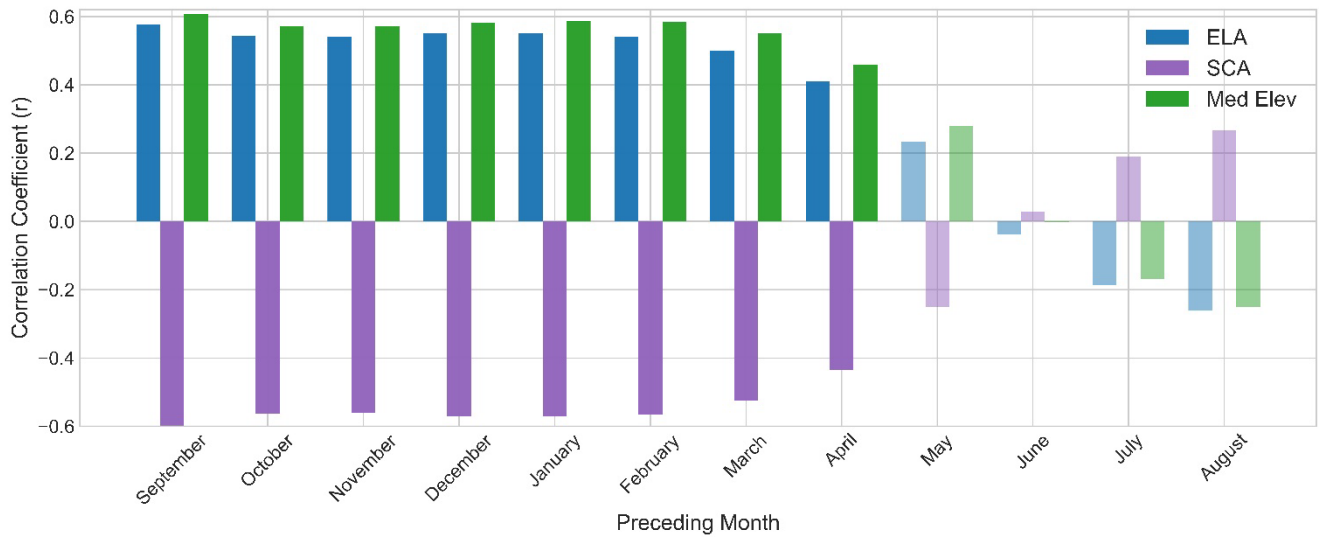


Figure 5: Zero-order correlations (r) for QIC variables (ELA, SCA, and Median Elevation (Med Elev)) and the ONI Index. Correlation coefficients with non-statistically significant p -values (>0.05) are denoted as semitransparent bars.

4 Discussion

4.1 QIC Response to Short-Term Climate Variability

During El Niño events the Peruvian Andes are often drier than average (Sulca et al., 2018), with on-site measurements at Quelccaya recording warmer and drier conditions (J. Hurley et al., 2019). To be considered an El Niño event, the SST anomalies must be high for at least four consecutive months (Lagos et al., 2008). Our results suggest these longer-term SST anomalies have a greater influence on the SCA than precipitation (i.e., no correlation is observed between wet season precipitation and the SCA, ELA, and SCA median elevation). We demonstrate that the El Niño events in 1998 and 2016 correspond to large reductions in QIC's SCA (Fig. 6). These SCA perturbations are outliers from the mean SCA (z -score = -2.3 and -2.11, respectively; avg z -score = 0.12). These are evident in QIC shallow ice cores which display a 'smoothed' $\delta^{18}\text{O}$ signal during the El Niño instead of the usual high-resolution variability, indicating warm and dry conditions that lack accumulation and experience melt (Thompson et al., 2017). Linear regression analysis with and without El Niño event years show differing slope coefficients, indicating these events are associated with an enhanced reduction in QIC SCA. As noted in the results, the SCA rebound from the 2016 El Niño did not fully occur until years later, unlike in 1999 which was one of the strongest La Niña events (ONI Index of -1.5) within the observation period, along with 1989 and 2011. This suggests the timing and magnitude of La Niña events are an additional factor influencing the year-to-year variability in SCA.

If we consider El Niño and La Niña events that correspond to ONI indexes greater than ± 1.0 , the linear regression model with an El Niño binary predictor shows a strong and significant relationship between TA and year ($R^2 = 0.94$, $p < 0.001$). However, variance analysis across the entire temporal scale indicates that El Niño years have a stronger impact on SCA, AAR, and ELA than on TA (Fig. S4, Table S4). While the SCA is notably briefly impacted by these El Niño events, decline from anthropogenic warming has resulted in the long-term decline of the SCA and TA of the QIC (Bradley et al., 2009; Rounce et al., 2023; Thompson et al., 2021; Vuille et al., 2018; Yarleque et al., 2018). Further, during all previously noted La Niña events (Fig. 6), the SCA experienced some level of temporary expansion, but throughout the 2021-2022 La Niña, the SCA did not rebound, but only declined further. While this is only one incidence, we expect this behavior to continue through the onset of the predicted upcoming 2024/2025 La Niña. The decrease in the percentage of days at or below freezing during the wet season will only exacerbate the decline in SCA. In addition, a recent study has projected faster onset and slower decline of future El Niños (Lopez et al., 2022). Considering the current state of the QIC and the ongoing El Niño, a slow decline of the current event will only delay recovery of the SCA, and act to enhance mass loss.

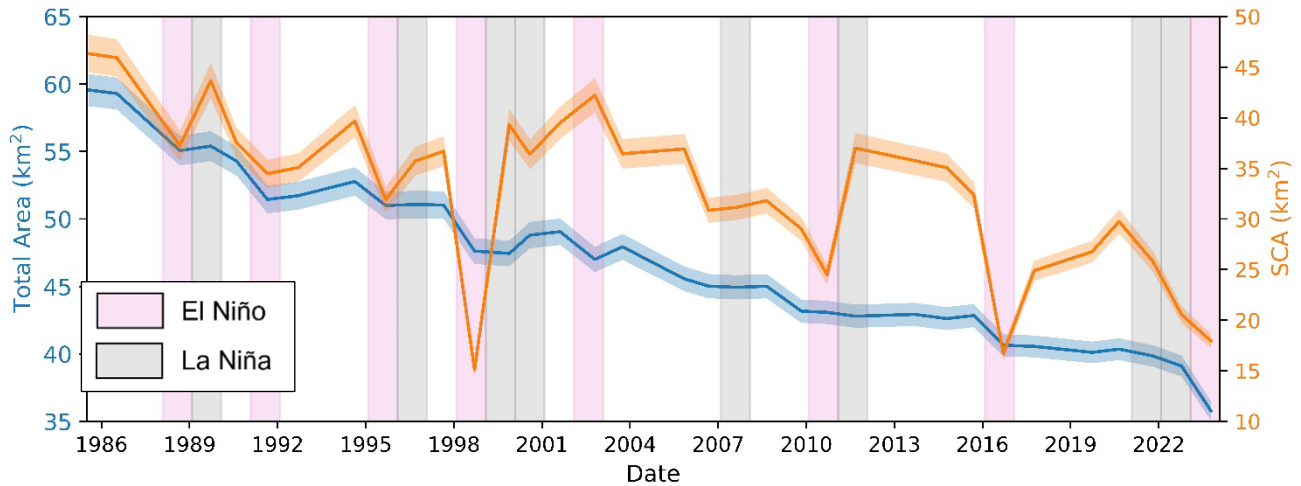


Figure 6: Decline of QIC's TA and SCA over the observational period (1985-2023). Timing of El Niño and La Niña events (with ONI indexes greater than ± 1.0) are noted in pink and gray colored bars, respectively.

4.2 Equilibrium State of the QIC

Glaciers in other locations such as the New Zealand Alps and the European Alps are considered in steady state with AARs of around 0.6 (Benn & Lehmkuhl, 2000), but tropical glaciers require an AAR of ~ 0.8 (Kaser & Osmaston, 2002). Discounting El Niño years (1998, 2016, and 2023), the QIC average AAR is 0.74, indicating the QIC is out of equilibrium, and likely somewhat lagging in response compared with the pace of ongoing climate change. The ice cap is pushed even more noticeably out of equilibrium during the observed El Niño events with AARs of 0.31, 0.41, and 0.53. These are far lower values than required for even high latitude glaciers, and far below the average for the QIC. Our results indicate the SCA has changed more dramatically on a year-to-year basis than the TA (Fig. 6), indicating rapid response of the SCA and thus the ELA to short-term climate variability, in addition to decadal-scale changes (Zekollari et al., 2020). This is consistent with other studies that indicate the QIC is likely responding to climate drivers within a few decades from the present, including the almost immediate response to El Niño events (Thompson, 2017; Veettil et al., 2017). Previous work on Quelccaya showed the median elevation of the entire QIC rose ~ 1.59 m per decade from 1975 to 2010 (Taylor et al., 2022), which is slightly less than our estimate (~ 1.91 m/decade), although we note the different temporal scale. Similarly, previous studies of the QIC note a mean ELA between 1992 and 2017 of $\sim 5,436$ m a.s.l. (Yarleque et al., 2018) while our automated methods suggest a mean ELA of $\sim 5,351$ m a.s.l. for the same temporal scale. Considering the QIC's out of equilibrium state, as well as continued decline of the SCA and rise of the ELA due to ongoing anthropogenic climate change, we suggest that the QIC will lose its SCA before 2080 (becoming a wasting ice field) and may completely melt away prior to 2100 (assuming the rate of loss is constant; Fig. S5). However, with increasing ice loss, there is potential for an uneven ice surface with standing water to change the albedo, and thus affect the QIC's mass balance, enhancing its decline (Naegeli & Huss, 2017; Wang et al., 2015).

345 **5 Conclusion**

We automate the process of satellite-based collection of yearly QIC variables important for mass balance assessment and assess the ice cap's short-term fluctuations to local climate forcings, including temperature fluctuations and El Niño events. We observe decadal-scale change in TA, SCA, and ELA and high interannual variability in SCA and ELA. Specifically, we observe staggering change in the QIC over the last four decades including a ~42% loss in TA, a ~61% loss in SCA, and a ~224
350 meter rise of the ELA. In the height of the wet season, the ONI index is significantly correlated with the QIC's SCA at the end of dry season, with noticeable decreases of the AAR during each El Niño event. While the SCA has responded rapidly to the ONI changes of the past, the SCA has declined through the most recent La Niña and may continue to do so during the next. Continued monitoring of the QIC will be vital, as the potential for surface processes and future El Niños to accelerate the ice loss rises with continued warming. Further, the QIC's future demise points towards water scarcity for the local population,
355 creating uncharted difficulties, especially seasonally (Veettil et al., 2017; Vuille et al., 2018).

Code and Data Availability

All calculated QIC variables from this study are provided within the supplementary information, detailed in Table S2. Annual SCA shapefile data and DEM bin distribution initially calculated within GEE is available at the following repository at
360 <https://doi.org/10.5281/zenodo.11265568>. A sample code for preprocessing and processing Landsat 8 images is available at the following url: <https://code.earthengine.google.com/cfcbd0780ff3f09b0698035cd6dd678a>.

Author Contribution

K.A.L. designed the study, developed the code, collected the snow cover data, and completed the analysis of the data and
365 accompanying climate variables. K.A.L. wrote the manuscript. K.A.L., L.J.L., L.G.T., and B.G.M. contributed to the discussion of the results, editing, and revision of the manuscript.

Competing Interests

The authors declare that they have no conflict of interest.
370

Acknowledgments

This research was supported by the Heising-Simons Foundation and Volo Foundation for both past field data used as reference and in support of the current project. We would like to thank the National Science Foundation (NSF) for graduate student support under Award #1805819. Additionally, we thank James Lea for providing GEE assistance with topographic corrections,
375 Rainey Aberle for providing guidance regarding ELA calculations, and Shelby Turner for insights into their climate projections in the Peruvian Andes. This is Byrd Polar and Climate Research Center contribution No. 1630.

References

- Benn, D. I., & Lehmkuhl, F. (2000). Mass balance and equilibrium-line altitudes of glaciers in high-mountain environments. *Quaternary International*, 65, 15–29.
- 380 Bradley, R. S., Keimig, F. T., Diaz, H. F., & Hardy, D. R. (2009). Recent changes in freezing level heights in the Tropics with implications for the deglaciation of high mountain regions. *Geophysical Research Letters*, 36(17), 2009GL037712. <https://doi.org/10.1029/2009GL037712>
- Bradley, R. S., Vuille, M., Diaz, H. F., & Vergara, W. (2006). Threats to water supplies in the tropical Andes. *Science*, 312(5781), 1755–1756.
- 385 Braun, M. H., Malz, P., Sommer, C., Fariás-Barahona, D., Sauter, T., Casassa, G., Soruco, A., Skvarca, P., & Seehaus, T. C. (2019). Constraining glacier elevation and mass changes in South America. *Nature Climate Change*, 9(2), 130–136.
- Brecher, H. H., & Thompson, L. G. (1993). Measurement of the Retreat of Qori Kalis Glacier in the Tropical Andes of Peru. *Terrestrial Photogrammetry*.
- Casimiro, W.S.L., Labat, D., Ronchail, J., Espinoza, J. C., & Guyot, J. L. (2013). Trends in rainfall and temperature in the Peruvian Amazon–Andes basin over the last 40 years (1965–2007). *Hydrological Processes*, 27(20), 2944–2957.
- 390 Dozier, J. (1989). Spectral signature of alpine snow cover from the Landsat Thematic Mapper. *Remote Sensing of Environment*, 28, 9–22.
- Ekstrand, S. (1996). Landsat TM-based forest damage assessment: Correction for topographic effects. *Photogrammetric Engineering and Remote Sensing*, 62(2), 151–162.
- 395 Fang, H., Baiping, Z., Yonghui, Y., Yunhai, Z., & Yu, P. (2011). Mass Elevation Effect and Its Contribution to the Altitude of Snowline in the Tibetan Plateau and Surrounding Areas. *Arctic, Antarctic, and Alpine Research*, 43(2), 207–212. <https://doi.org/10.1657/1938-4246-43.2.207>
- Favier, V., Wagnon, P., & Ribstein, P. (2004). Glaciers of the outer and inner tropics: A different behaviour but a common response to climatic forcing. *Geophysical Research Letters*, 31(16).
- 400 Gaddam, V. K., Boddapati, R., Kumar, T., Kulkarni, A. V., & Bjornsson, H. (2022). Application of “OTSU”—An image segmentation method for differentiation of snow and ice regions of glaciers and assessment of mass budget in Chandra basin, Western Himalaya using Remote Sensing and GIS techniques. *Environmental Monitoring and Assessment*, 194(5), 337. <https://doi.org/10.1007/s10661-022-09945-2>
- Ge, H., Lu, D., He, S., Xu, A., Zhou, G., & Du, H. (2008). Pixel-based Minnaert Correction Method for Reducing Topographic Effects on a Landsat 7 ETM+ Image. *Photogrammetric Engineering & Remote Sensing*, 74(11), 1343–1350. <https://doi.org/10.14358/PERS.74.11.1343>
- Hall, D. K., & Riggs, G. A. (2007). Accuracy assessment of the MODIS snow products. *Hydrological Processes*, 21(12), 1534–1547.
- Hanshaw, M. N., & Bookhagen, B. (2014). Glacial areas, lake areas, and snow lines from 1975 to 2012: Status of the Cordillera Vilcanota, including the Quelccaya Ice Cap, northern central Andes, Peru. *The Cryosphere*, 8(2), 359–376. <https://doi.org/10.5194/tc-8-359-2014>
- 410 Hu, Z., Dietz, A., Zhao, A., Ureyen, S., Zhang, H., Wang, M., Mederer, P., & Kuenzer, C. (2020). Snow Moving to Higher Elevations: Analyzing Three Decades of Snowline Dynamics in the Alps. *Geophysical Research Letters*, 47(12), e2019GL085742. <https://doi.org/10.1029/2019GL085742>
- 415 Hugonnet, R., McNabb, R., Berthier, E., Menounos, B., Nuth, C., Girod, L., Farinotti, D., Huss, M., Dussaillant, I., Brun, F., & Käab, A. (2021). Accelerated global glacier mass loss in the early twenty-first century. *Nature*, 592(7856), 726–731. <https://doi.org/10.1038/s41586-021-03436-z>
- Hurley, J. V., Vuille, M., Hardy, D. R., Burns, S. J., & Thompson, L. G. (2015). Cold air incursions, $\delta^{18}\text{O}$ variability, and monsoon dynamics associated with snow days at Quelccaya Ice Cap, Peru. *Journal of Geophysical Research: Atmospheres*, 120(15), 7467–7487. <https://doi.org/10.1002/2015JD023323>
- 420 Hurley, J., Vuille, M., & Hardy, D. R. (2019). On the interpretation of the ENSO signal embedded in the stable isotopic composition of Quelccaya Ice Cap, Peru. *Journal of Geophysical Research: Atmospheres*, 124(1), 131–145.
- Kaser, G., & Osmaston, H. (2002). *Tropical glaciers*. Cambridge University Press.

- 425 Klein, A. G., & Isacks, B. L. (1999). Spectral mixture analysis of Landsat thematic mapper images applied to the detection of the transient snowline on tropical Andean glaciers. *Global and Planetary Change*, 22(1–4), 139–154. [https://doi.org/10.1016/S0921-8181\(99\)00032-6](https://doi.org/10.1016/S0921-8181(99)00032-6)
- Lamantia, K., Thompson, L., Davis, M., Mosley-Thompson, E., & Stahl, H. (2023). Unique Collections of ¹⁴C-Dated Vegetation Reveal Mid-Holocene Fluctuations of the Quelccaya Ice Cap, Peru. *Journal of Geophysical Research: Earth Surface*, 128(11), e2023JF007297. <https://doi.org/10.1029/2023JF007297>
- 430 Li, X., Wang, N., & Wu, Y. (2022). Automated Glacier Snow Line Altitude Calculation Method Using Landsat Series Images in the Google Earth Engine Platform. *Remote Sensing*, 14(10), 2377. <https://doi.org/10.3390/rs14102377>
- Liu, C., Li, Z., Zhang, P., Tian, B., Zhou, J., & Chen, Q. (2021). Variability of the snowline altitude in the eastern Tibetan Plateau from 1995 to 2016 using Google Earth Engine. *Journal of Applied Remote Sensing*, 15(04). <https://doi.org/10.1117/1.JRS.15.048505>
- 435 Lopez, H., Lee, S.-K., Kim, D., Wittenberg, A. T., & Yeh, S.-W. (2022). Projections of faster onset and slower decay of El Niño in the 21st century. *Nature Communications*, 13(1), 1915.
- Mark, B. G., Seltzer, G. O., Rodbell, D. T., & Goodman, A. Y. (2002). Rates of Deglaciation during the Last Glaciation and Holocene in the Cordillera Vilcanota-Quelccaya Ice Cap Region, Southeastern Perú. *Quaternary Research*, 57(3), 287–298. <https://doi.org/10.1006/qres.2002.2320>
- 440 Meier, M. F. (1962). Proposed definitions for glacier mass budget terms. *Journal of Glaciology*, 4(33), 252–263.
- Naegeli, K., & Huss, M. (2017). Sensitivity of mountain glacier mass balance to changes in bare-ice albedo. *Annals of Glaciology*, 58(75pt2), 119–129.
- Paul, F., Barrand, N. E., Baumann, S., Berthier, E., Bolch, T., Casey, K., Frey, H., Joshi, S., Konovalov, V., & Le Bris, R. (2013). On the accuracy of glacier outlines derived from remote-sensing data. *Annals of Glaciology*, 54(63), 171–182.
- 445 Pepin, N., Arnone, E., Gobiet, A., Haslinger, K., Kotlarski, S., Notarnicola, C., Palazzi, E., Seibert, P., Serafin, S., & Schöner, W. (2022). Climate changes and their elevational patterns in the mountains of the world. *Reviews of Geophysics*, 60(1), e2020RG000730.
- Pepin, N., Bradley, R. S., Diaz, H. F., Baraer, M., Caceres, E. B., Forsythe, H., Fowler, G., Greenwood, G., Hasmi, M. Z., Liu, X. D., Miller, J. R., Ning, L., Ohmura, A., Palazzi, E., Rangwala, I., Schöner, S., Severskiy, I., Shahgedanova, M., Wang, M. B., ... Yang, D. Q. (2015). Elevation-dependent warming in mountain regions of the world. *Nature Climate Change*, 5(5), 424–430.
- Rabatel, A., Bermejo, A., Loarte, E., Soruco, A., Gomez, J., Leonardini, G., Vincent, C., & Sicart, J. E. (2012). Can the snowline be used as an indicator of the equilibrium line and mass balance for glaciers in the outer tropics? *Journal of Glaciology*, 58(212), 1027–1036.
- 455 Rabatel, A., Francou, B., Soruco, A., Gomez, J., Cáceres, B., Ceballos, J. L., Basantes, R., Vuille, M., Sicart, J.-E., & Huggel, C. (2013). Current state of glaciers in the tropical Andes: A multi-century perspective on glacier evolution and climate change. *The Cryosphere*, 7(1), 81–102.
- Racoviteanu, A. E., Rittger, K., & Armstrong, R. (2019). An Automated Approach for Estimating Snowline Altitudes in the Karakoram and Eastern Himalaya From Remote Sensing. *Frontiers in Earth Science*, 7, 220. <https://doi.org/10.3389/feart.2019.00220>
- 460 Rounce, D. R., Hock, R., Maussion, F., Hugonnet, R., Kochtitzky, W., Huss, M., Berthier, E., Brinkerhoff, D., Compagno, L., & Copland, L. (2023). Global glacier change in the 21st century: Every increase in temperature matters. *Science*, 379(6627), 78–83.
- 465 Sankey, T., Donald, J., McVay, J., Ashley, M., O'Donnell, F., Lopez, S. M., & Springer, A. (2015). Multi-scale analysis of snow dynamics at the southern margin of the North American continental snow distribution. *Remote Sensing of Environment*, 169, 307–319.
- Schauwecker, S., Rohrer, M., Acuña, D., Cochachin, A., Dávila, L., Frey, H., Giráldez, C., Gómez, J., Huggel, C., Jacques-Coper, M., Loarte, E., Salzmann, N., & Vuille, M. (2014). Climate trends and glacier retreat in the Cordillera Blanca, Peru, revisited. *Global and Planetary Change*, 119, 85–97. <https://doi.org/10.1016/j.gloplacha.2014.05.005>
- 470 Seehaus, T., Malz, P., Sommer, C., Soruco, A., Rabatel, A., & Braun, M. (2020). Mass balance and area changes of glaciers in the Cordillera Real and Tres Cruces, Bolivia, between 2000 and 2016. *Journal of Glaciology*, 66(255), 124–136.

- 475 Sulca, J., Takahashi, K., Espinoza, J., Vuille, M., & Lavado-Casimiro, W. (2018). Impacts of different ENSO flavors and tropical Pacific convection variability (ITCZ, SPCZ) on austral summer rainfall in South America, with a focus on Peru. *International Journal of Climatology*, *38*(1), 420–435.
- Taylor, L. S., Quincey, D. J., Smith, M. W., Potter, E. R., Castro, J., & Fyffe, C. L. (2022). Multi-Decadal Glacier Area and Mass Balance Change in the Southern Peruvian Andes. *Frontiers in Earth Science*, *10*.
- Thompson, L. G. (2000). Ice core evidence for climate change in the Tropics: Implications for our future. *Quaternary Science Reviews*, *19*(1–5), 19–35. [https://doi.org/10.1016/S0277-3791\(99\)00052-9](https://doi.org/10.1016/S0277-3791(99)00052-9)
- 480 Thompson, L. G. (2017). Past, present, and future of glacier archives from the world’s highest mountains. *Proceedings of the American Philosophical Society*, *161*(3), 226–243.
- Thompson, L. G., Davis, M. E., Mosley-Thompson, E., Beaudon, E., Porter, S. E., Kutuzov, S., Lin, P. -N., Mikhailenko, V. N., & Mountain, K. R. (2017). Impacts of Recent Warming and the 2015/2016 El Niño on Tropical Peruvian Ice Fields. *Journal of Geophysical Research: Atmospheres*, *122*(23). <https://doi.org/10.1002/2017JD026592>
- 485 Thompson, L. G., Davis, M. E., Mosley-Thompson, E., Porter, S. E., Corrales, G. V., Shuman, C. A., & Tucker, C. J. (2021). The impacts of warming on rapidly retreating high-altitude, low-latitude glaciers and ice core-derived climate records. *Global and Planetary Change*, *203*, 103538. <https://doi.org/10.1016/j.gloplacha.2021.103538>
- Thompson, L. G., Mosley-Thompson, E., Bolzan, J. F., & Koci, B. R. (1985). A 1500-Year Record of Tropical Precipitation in Ice Cores from the Quelccaya Ice Cap, Peru. *Science*, *229*(4717). <https://doi.org/10.1126/science.229.4717.971>
- 490 Thompson, L. G., Mosley-Thompson, E., Davis, M. E., & Brecher, H. H. (2011). Tropical glaciers, recorders and indicators of climate change, are disappearing globally. *Annals of Glaciology*, *52*(59), 23–34. <https://doi.org/10.3189/172756411799096231>
- Thompson, L. G., Mosley-Thompson, E., Davis, M. E., Zagorodnov, V. S., Howat, I. M., Mikhailenko, V. N., & Lin, P.-N. (2013). Annually Resolved Ice Core Records of Tropical Climate Variability over the Past ~1800 Years. *Science*, *340*(6135). <https://doi.org/10.1126/science.1234210>
- 495 Veettil, B. K., Wang, S., Florêncio de Souza, S., Bremer, U. F., & Simões, J. C. (2017). Glacier monitoring and glacier-climate interactions in the tropical Andes: A review. *Journal of South American Earth Sciences*, *77*, 218–246. <https://doi.org/10.1016/j.jsames.2017.04.009>
- Vuille, M., Bradley, R. S., & Keimig, F. (2000). Interannual climate variability in the Central Andes and its relation to tropical Pacific and Atlantic forcing. *Journal of Geophysical Research: Atmospheres*, *105*(D10), 12447–12460. <https://doi.org/10.1029/2000JD900134>
- Vuille, M., Carey, M., Huggel, C., Buytaert, W., Rabatel, A., Jacobsen, D., Soruco, A., Villacis, M., Yarleque, C., Elison Timm, O., Condom, T., Salzmann, N., & Sicart, J.-E. (2018). Rapid decline of snow and ice in the tropical Andes – Impacts, uncertainties and challenges ahead. *Earth-Science Reviews*, *176*, 195–213. <https://doi.org/10.1016/j.earscirev.2017.09.019>
- 505 Vuille, M., Franquist, E., Garreaud, R., Lavado Casimiro, W. S., & Cáceres, B. (2015). Impact of the global warming hiatus on Andean temperature. *Journal of Geophysical Research: Atmospheres*, *120*(9), 3745–3757.
- Vuille, M., Kaser, G., & Juen, I. (2008). Glacier mass balance variability in the Cordillera Blanca, Peru and its relationship with climate and the large-scale circulation. *Global and Planetary Change*, *62*(1–2), 14–28. <https://doi.org/10.1016/j.gloplacha.2007.11.003>
- 510 Wang, W., Xiang, Y., Gao, Y., Lu, A., & Yao, T. (2015). Rapid expansion of glacial lakes caused by climate and glacier retreat in the Central Himalayas. *Hydrological Processes*, *29*(6), 859–874.
- Yarleque, C., Vuille, M., Hardy, D. R., Timm, O. E., De la Cruz, J., Ramos, H., & Rabatel, A. (2018). Projections of the future disappearance of the Quelccaya Ice Cap in the Central Andes. *Scientific Reports*, *8*(1), 1–11.
- 515 Zekollari, H., Huss, M., & Farinotti, D. (2020). On the imbalance and response time of glaciers in the European Alps. *Geophysical Research Letters*, *47*(2), e2019GL085578.